JPE 12-3-11

http://dx.doi.org/10.6113/JPE.2012.12.3.477

Extension of the Operating Speed for Vector-Controlled Induction Machine Drives in the Overmodulation Range

Thanh Hai Nguyen* and Dong-Choon Lee†

†*Dept. of Electrical Engineering, Yeungnam University, Gyeongsan, Korea

Abstract

This paper proposes a novel current control scheme for vector-controlled induction machine (IM) drives in the overmodulation (OVM) range, with which the voltage utilization of the voltage-source inverter (VSI) can be maximized. In the OVM region, the original voltage reference is modified by changing its magnitude and angle, which causes the motor current to be distorted, resulting in a deterioration of the current control performance. To meet with this situation, the harmonic components in the feedback currents should be eliminated before being input to the PI current controllers. For this, a composite observer is applied to extract the fundamental and harmonic components from the distorted currents, which gives a good performance without a delay and the effect of a fundamental frequency variation. In addition, through a detailed analysis of the response of the PI current controllers in the OVM range, the effectiveness of using the composite observer is demonstrated. Simulation and experimental results for a 3-kW induction motor drive are shown to verify the validity of the proposed method.

Key Words: Composite observer, Induction machine drives, Overmodulation, PWM, Vector control

I. INTRODUCTION

A voltage-source inverter with a front-end diode rectifier shown in Fig. 1 is commonly used in variable-speed machine drive applications due to its low cost and high efficiency. For these applications with a fixed DC-link voltage, OVM techniques have been paid considerable attention for PWM-VSI, in which it provides full voltage utilization of the inverters for SVPWM (space-vector pulse-width modulation) [1]-[3].

In high-performance motor drive systems, fast torque control is an essential requirement. The vector control of AC machines is usually used for these applications, in which fast current control is necessary over a wide range of operations. The role of the current controllers is to generate the voltage reference for the inverter modulation, which makes the machine current follow the command. A proportional plus integral (PI) regulator is commonly used for the current control, which operates satisfactorily just for the DC quantities. The linear voltage range of a PWM-VSI is mainly considered. To utilize the input voltage of the inverter fully, the pulse-width modulator has to operate in the OVM range. For achieving this condition, the magnitude and phase of the reference voltage vector is modified [1]-[2], which causes the motor currents to be distorted [4]. The influence of these harmonics on the PI-type linear current controller is still a critical issue.

To overcome these drawbacks, several previous methods have been introduced with the goal of reducing the impacts of the current harmonics on the PI current controller. To eliminate the harmonic components in the feedback current, a low-pass filters (LPF) can be employed. However, the bandwidth of the current controllers is reduced. In addition, a band-pass filters (BPF) can be used to extract the harmonic components of the currents. However, the BPF may not perform well when the operating frequency drifts from the resonance frequency since the cut-off frequency of the BPF is fixed.

Another method for compensating the harmonic components in the feedback current has been proposed, where the first-order model was used to estimate the harmonic components [4]. This algorithm offered good performance for the vector control in the OVM range up to

Manuscript received Dec. 2, 2011; revised Feb. 27, 2012
Recommended for publication by Associate Editor Jang-Mok Kim.
†Corresponding Author: dclee@yu.ac.kr
Tel: +82-53-810-2582, Fax: +82-53-810-4767, Yeungnam University
*Dept. of Electrical Eng., Yeungnam University, Korea

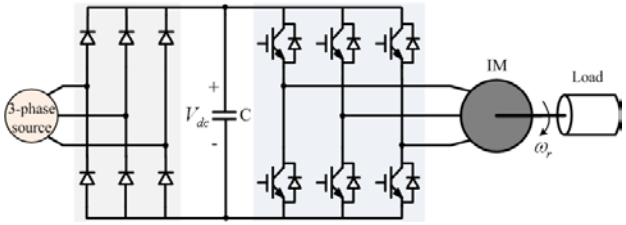

Fig. 1. Induction motor drive system.

the six-step mode. However, the machine parameters are needed to implement this algorithm. In addition, a method similar to [4] has been proposed for a sensorless vector controlled induction motor drive [5], where the difference is that the estimation is made in a stationary coordinate. The performance of the current controllers has been improved with a composite observer as presented in [6]. However, the validity of the algorithm has not been verified by experimental results. Some other studies have been introduced for vector-controlled machine drives in the OVM range [7]-[9], where the stator-flux-based SVPWM is applied. However, flux distortion and high torque pulsation of the machine appear. A method for control mode switching between vector control and constant *V/f* control in the OVM range has been introduced in [10]. However, during operation in the OVM range, the control scheme operates only in *V/f* mode.

The OVM strategies presented in [11]-[12] achieved better performance in the transient operation of machine drive applications. However, the problems in [11]-[13], which deal with the compensation of the dynamic voltage component during the OVM operation, are different from the problems addressed in this paper.

Fig. 2 shows the speed-torque characteristics of an IM driven by a PWM inverter. However, the steady-state operation of the conventional vector control works well only when the machine speed is less than the base speed, ω_{base}. Meanwhile, when applying the proposed strategy to vector-controlled induction machine drives, the rated machine torque can be kept when the machine speed is higher than the base speed.

A composite observer method is applied to estimate the DC-component and the multiples of 6^{th}-order harmonic component in the feedback currents of the PI current controllers. The online extraction using the composite observer offers good performance for the harmonics with a variation of the resonance frequency. The harmonic components in the feedback currents can be eliminated before being input to the PI current controllers. Therefore, the performance of the PI current controller can be improved.

The validity of the proposed method is verified by simulation and experimental results for a 3-kW induction motor drive.

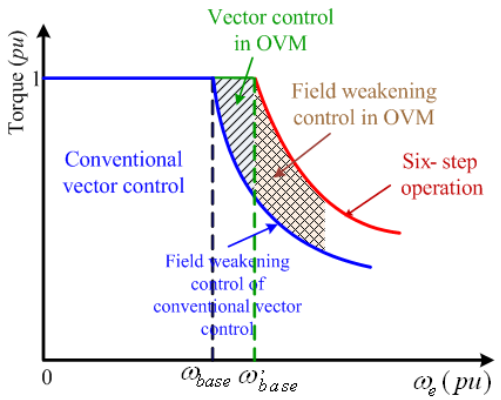

Fig. 2. Torque-speed characteristics of IM driven by PWM inverter.

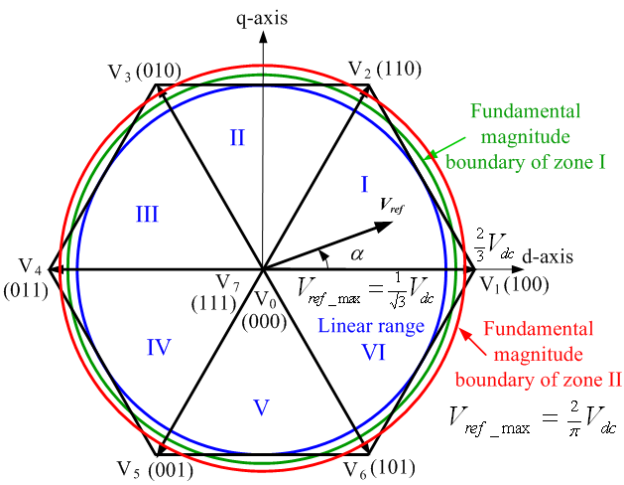

Fig. 3. Diagram of voltage vectors in linear and OVM modes.

II. Overmodulation Strategy for PWM Inverters

For the OVM schemes presented in [1]-[3], the fundamental output voltage of the inverters can be generated so that it is exactly equal to that of the reference voltage by the contribution of the voltage increments around each corner of the hexagon. Therefore, the modified reference voltage is determined based on a full fundamental cycle of the inverter output voltage. For this reason, these OVM techniques are called static OVM strategies in this paper. On the other hand, for the OVM techniques in [11]-[12], the reference voltage is modified based on every switching period, which are called dynamic OVM strategies.

A. Static OVM strategy

The modulation index of a PWM inverter is defined as the ratio of the peak value of the fundamental of the modulated

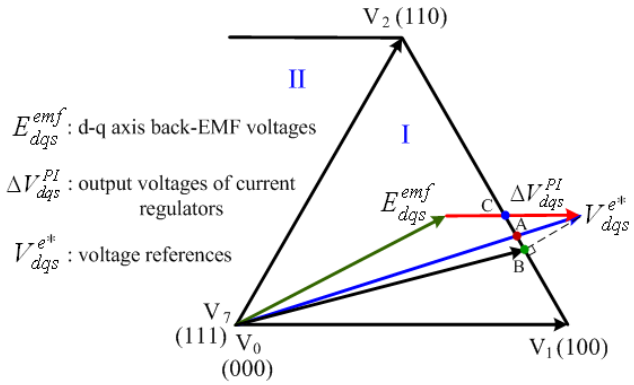

Fig. 4. Modified voltage reference in dynamic OVM strategy.

output voltage to that obtained in six-step mode operation, which is given by:

$$MI = \frac{V_{ref}}{\frac{2}{\pi}V_{dc}} \tag{1}$$

where V_{ref} is the magnitude of the phase voltage reference and V_{dc} is the inverter input voltage.

The maximum output voltage in the PWM inverter is obtained during the six-step operation in which the fundamental voltage component is $2V_{dc}/\pi$. In the linear control range, the maximum value of the fundamental component is $V_{dc}/\sqrt{3}$, in which the modulation index is 0.906.

The overmodulation range refers to the operation regions of the pulse-width modulator beyond the linear range which indicates the inscribed circle of the hexagon. According to the modulation index, the PWM range is divided into three regions as seen in Fig. 3 and described in detail in [1].

Linear modulation (0 ≤ MI ≤ 0.906): the space-vector modulator produces sinusoidal output voltages.

OVM mode I (0.906 < MI ≤ 0.952): a modified voltage vector reference is derived from the reference voltage vector by changing its magnitude, whereas the phase angle is kept at its original value.

OVM mode II (0.952 < MI ≤ 1): an actual voltage reference vector is kept at a vertex of the hexagon for a particular time and a change in the phase angle of the modified reference vector is required.

The modified voltage vector references for the two modes above have been described in detail in [1], [10].

B. Dynamic OVM strategies

The dynamic OVM strategies improve the performance of the current controllers in transient state.

Fig. 4 shows conventional dynamic OVM strategies where the voltage references are modified to be placed on the sides of hexagon [11]-[12]. The phase angle of the reference voltage is maintained by selecting a modified reference voltage at point A. Point B in Fig. 4 shows that the magnitude error between the original reference voltage and the modified one is minimized. The current error with consideration of the current transition is minimized by keeping the phase angle of the output voltage of the current regulator. Hence the modified reference voltage is determined at an intersection of the hexagon, and the current regulator output indicates point C in Fig. 4. However, these modified reference voltages are always less than that required of the PI current regulator, so the machine current control capability may be lost in steady-state operation.

III. Problems of Current Controllers in the OVM Range

In the OVM range, harmonic components of the output voltage exist, in which the even-order and triplen harmonic components are eliminated naturally in three-phase systems. Therefore, the harmonics of the 5th, 7th, 11th, 13th order, etc. are included in the output voltage of the PWM inverter, u^s, expressed in the stationary reference frame as:

$$u^s = u_1(e^{j\omega_e t} + H_5 e^{-j5\omega_e t} + H_7 e^{j7\omega_e t} + \\ + H_{11} e^{-j11\omega_e t} + H_{13} e^{j13\omega_e t} + \cdots) \tag{2}$$

where u_1 is the fundamental output voltage component and H_k (k=5, 7, 11, 13, …) is the ratio of the k^{th} harmonic component and its fundamental.

When the inverter output voltage is fed to the machine, the harmonic voltages cause the harmonic currents in the machine, which is expressed as:

$$i^s = i_1(e^{j\omega_e t} + H_{i5} e^{-j5\omega_e t} + H_{i7} e^{j7\omega_e t} + \\ + H_{i11} e^{-j11\omega_e t} + H_{i13} e^{j13\omega_e t} + \cdots) \tag{3}$$

where i^s is the machine current vector in the stationary reference frame, i_1 is the fundamental current component, and H_{ik} (k=5, 7, 11, 13, …) is the ratio of the k^{th} harmonic current components to its fundamental value.

For vector-controlled machine drives, the current controller is usually implemented in the rotating reference frame. The machine current vector, i^e, can be expressed in the synchronous reference frame as:

$$\begin{aligned} i^e &= i^s \cdot e^{-j\omega_e t} \\ &= i_1(1 + H_{i5} e^{-j6\omega_e t} + H_{i7} e^{j6\omega_e t} + \\ &\quad + H_{i11} e^{-j12\omega_e t} + H_{i13} e^{j12\omega_e t} + \cdots) \end{aligned} \tag{4}$$

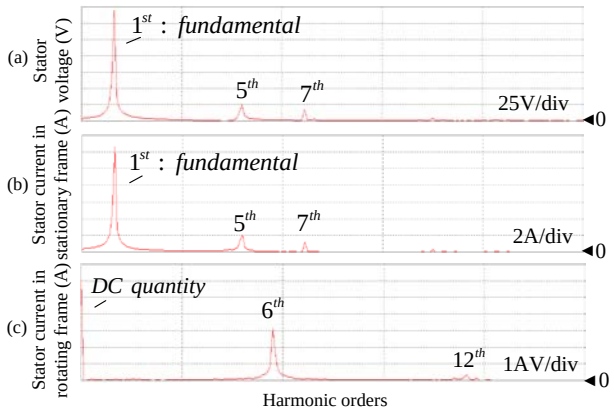

Fig. 5. Harmonic spectra by FFT.
(a) Stator voltage. (b) Stator current in stationary reference frame. (c) Stator current in synchronous reference frame.

Then, the machine currents are transformed into a DC quantity and multiples of the 6th-order harmonic components. Fig. 5 shows the machine current and the inverter output voltage through the FFT (fast Fourier transform). Fig. 5(a) shows the stator voltage composed of the fundamental and high-order components of the 5th and 7th. The stator current also included the high-order components, as shown in Fig. 5(b). It can be seen in Fig. 5(c) that the DC component and the multiples of the 6th-order harmonics only exist in the synchronous reference frame of the stator current. As an example, the 6th order harmonic current of machines operating at a rated frequency of 60Hz will be excited by PI controllers with a high bandwidth of 400 Hz. Hence the performance of the PI current controllers is severely deteriorated, even during steady-state operation.

The output voltage of the inverters applying the sampling time-based OVM strategies cannot be boosted high enough to achieve the operation area, as shown in Fig. 2.

IV. Proposed Current Control Strategy in the OVM Range

For the vector control method, the PI linear current controller is properly implemented for the machine current space vector in the synchronous reference frame since only the DC quantity exists. However, as described in section III, the presence of multiples of the 6th-order harmonics in the feedback currents in OVM range operation significantly degrades the performance of the PI current controllers.

To improve the performance of the current controller in the OVM ranges, the multiples of the 6th-order harmonics of the feedback currents in the synchronous reference frame need to be eliminated. To do this, a composite observer is applied to extract the DC and the multiples of the 6th-order harmonic components of the feedback currents, where

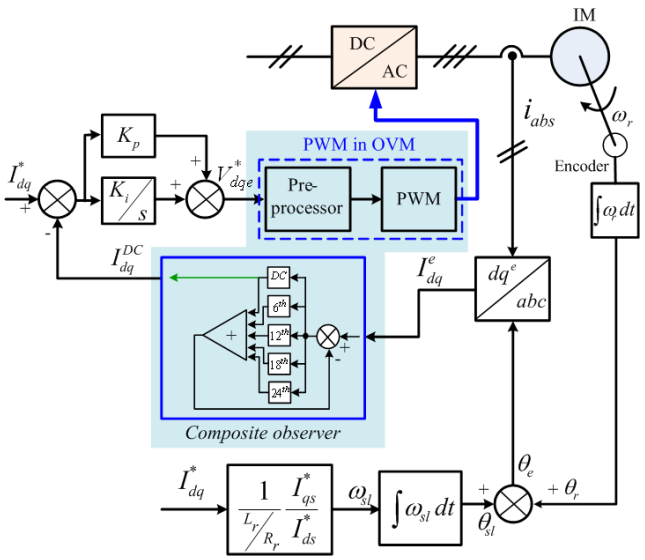

Fig. 6. Control block diagram of the current controller in OVM range.

applications and the performance of the composite observer have been illustrated in [14]-[16].

Under a rated load condition, the OVM occurs when the synchronous speed of the motor is higher than the base speed ω_{base}, as can be seen in Fig. 2. The base speed, where the field weakening operation of the machines begins, is decided by the voltage and the current constrains as [17]-[18]:

$$\omega_{base} = \frac{V_{s,\max}}{\sqrt{\lambda_{r,mag}^2 \dfrac{L_s^2 - (\sigma L_s)^2}{L_m^2} + (\sigma L_s I_{s,rated})^2}} \quad (5)$$

where $V_{s,\max}$ is the maximum fundamental magnitude of the inverter output voltage ($V_{s,\max} = V_{dc}/\sqrt{3}$ in the linear range), $I_{s,rated}$ is the magnitude of the rated stator current, $\lambda_{r,mag}$ is the rated machine flux, L_m and L_s are the magnetizing and stator leakage inductances, and σ is the leakage factor. When the operating speed is within the range of $\omega_{base} \sim \omega'_{base}$, the rated torque is maintained by the OVM operation of the inverter. Under the OVM range, the maximum of the fundamental component can be obtained as follows:

$$V_{s,\max}^{OVM} = 2V_{dc}/\pi . \quad (6)$$

Hence, the maximum operating speed can be increased in the OVM operation as:

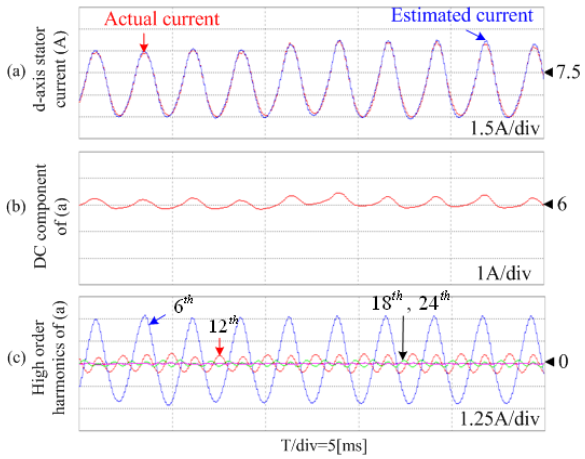

Fig. 7. Performance of composite observer (MI=0.992).
(a) Actual and estimated currents, (b) Estimated DC component, (c) k·6th order harmonic components (k=1~4).

$$\omega_{base}^{'} = \frac{V_{s,\max}^{OVM}}{V_{s,\max}} \omega_{base} = 1.103\omega_{base}. \qquad (7)$$

This indicates that the operating speed can be increased up to 10.3% higher than that of the conventional current controller of vector-controlled induction machine drives.

Fig. 6 shows a block diagram of a vector-controlled induction motor drive with a composite observer for harmonic current estimation. The composite observer provides a highly accurate extraction without a delay. In addition, its performance is not degraded when the machine current frequency deviates during variations of the machine speed. The measured currents are transformed to the *dq*-axis components in the synchronous reference frame. Then, the DC signals of the components extracted by the composite observer are fed to the controllers. For this observer, the fundamental frequency of the composite observer is set as 60 Hz. The 6th, 12th, 18th, and 24th order components are considered for the estimation.

The reference voltages which are the output of the PI current controllers are pre-processed by the static OVM strategy. Then, the modified reference voltages are generated by the PWM inverter.

For the current controller, the PI controller gains, K_P and K_i, have been chosen as:

$$\begin{aligned} K_p &= 0.5 \cdot L_{trans}\omega_c \\ K_i &= 0.5 \cdot R_{trans}\omega_c \end{aligned} \qquad (8)$$

where R_{trans} and L_{trans} are the equivalent stator resistance and the transient stator inductance. $\omega_c = 3000[rad/s]$ in this study.

TABLE I
PARAMETERS OF INDUCTION MACHINE

Rated power	3 kW
Stator voltage/frequency	220 V/60 Hz
Stator resistance	0.533 Ω
Rotor resistance	0.93 Ω
Stator/rotor inductance	3 mH
Magnetizing inductance	76 mH
Number of poles	4
Motor inertia	0.0033[kg.m^2]

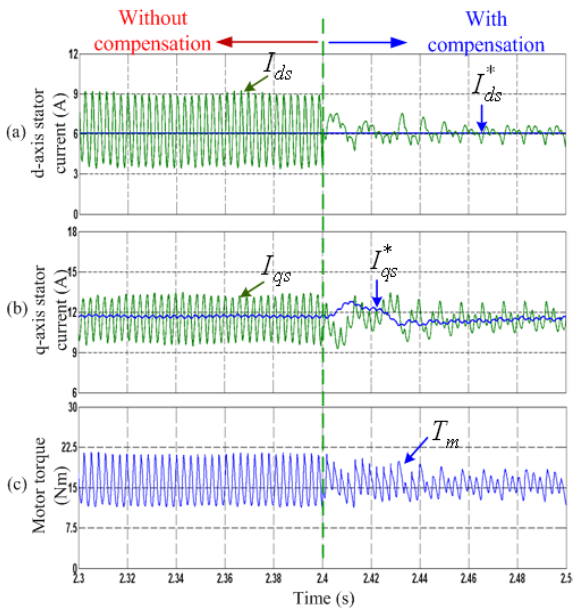

Fig. 8. Performance comparison of PI current controllers (MI=0.987).
(a) d-axis current. (b) q-axis current. (c) Motor torque.

The PI controller gains are lower than those of the linear range of the PWM operation to reduce the overshoot of the current controller response at the corner of the hexagon.

V. SIMULATION RESULTS

To verify the effectiveness of the proposed method, a PSIM simulation has been carried out for a 3-kW IM drive model under a full load condition. The machine parameters are listed in the Table I. The inverter input voltage provided by a front-end diode rectifier is 285V to generate the OVM operation conditions. A full load condition of 15.7 Nm is applied to the motor. From the parameters of the test system, the base speed of the motor is determined as 341.3 rad/s by (5), which gives an equivalent mechanical speed of 1,524 rpm.

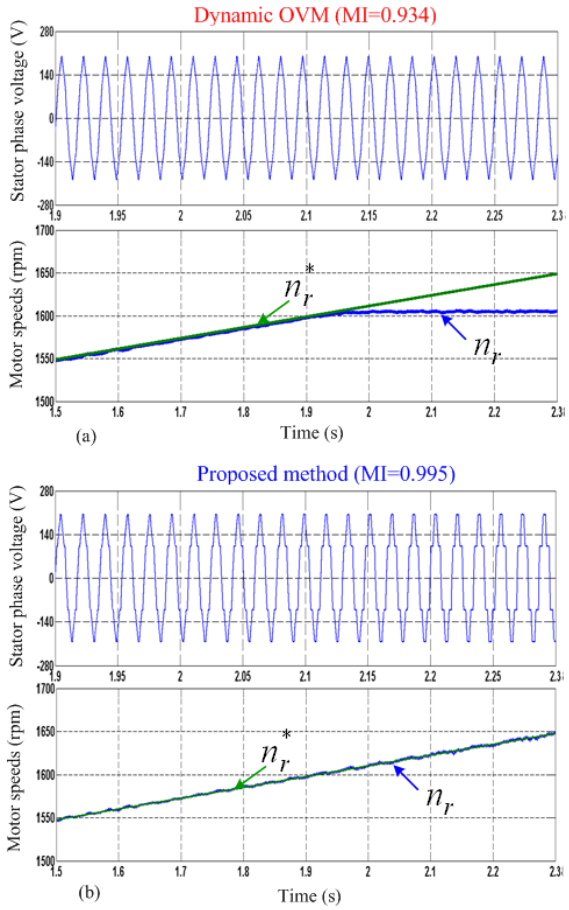

Fig. 9. Performance comparison of OVM strategies.
(a) Stator voltage and machine speed with dynamic OVM.
(b) Stator voltage and machine speed with the proposed method.

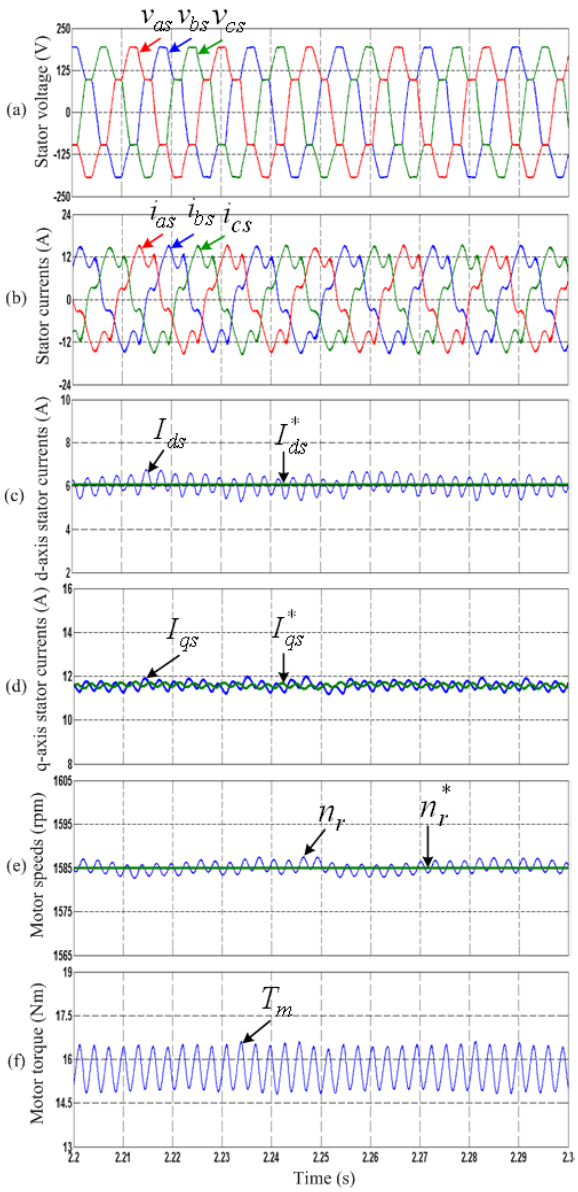

Fig. 10. Performance of the machine under OVM range (MI=0.985).
(a) Stator phase voltage. (b) Stator phase currents. (c) d-axis currents. (d) q-axis currents. (e) Speeds. (f) Torque.

The simulation conditions are listed as follows. The switching frequency of the inverter is 5 kHz, so the sampling time of the current controller is set to 100 μs. In addition, the control bandwidth of the current controller is set to 500 Hz. For the discrete observer design, the nominal frequency is chosen as the rated frequency of the machine, 60 Hz. The sampling period is also 100 μs. For a frequency deviation due to the variation of operating motor speed by ±10%, the observer performance is still good [15]-[16].

Fig. 7 shows the performance of the motor current estimation by the composite observer, in which the machine operates under the full load condition and at a speed of 1,610 rpm. Fig. 7(a) shows the actual and estimated currents in the synchronous reference frame, in which the estimated current is almost the same as the actual one. The estimated DC component of the machine current is shown in Fig. 7(b) and the harmonic components such as the 6th, 12th, 18th, and 24th are shown in Fig. 7(c). The 18th and 24th harmonics are almost zero.

Fig. 8 shows a comparison of the current control performances between the conventional method (without harmonic current elimination) and the proposed one under the full load condition, where the MI of the inverter is 0.987 and the machine speed is 1,590 rpm. The performance of the current controller with harmonic compensation is much better. The ripple components of the *dq*-axis currents are significantly reduced, as shown in Fig. 8(a) and (b). This results in a reduction of the torque ripple in the machine when compared to that without harmonic compensation, as shown in Fig. 8(c).

Fig. 9 shows a comparison of the machine drive performance in the cases of the dynamic OVM and the static OVM for the current control. The waveforms of the stator

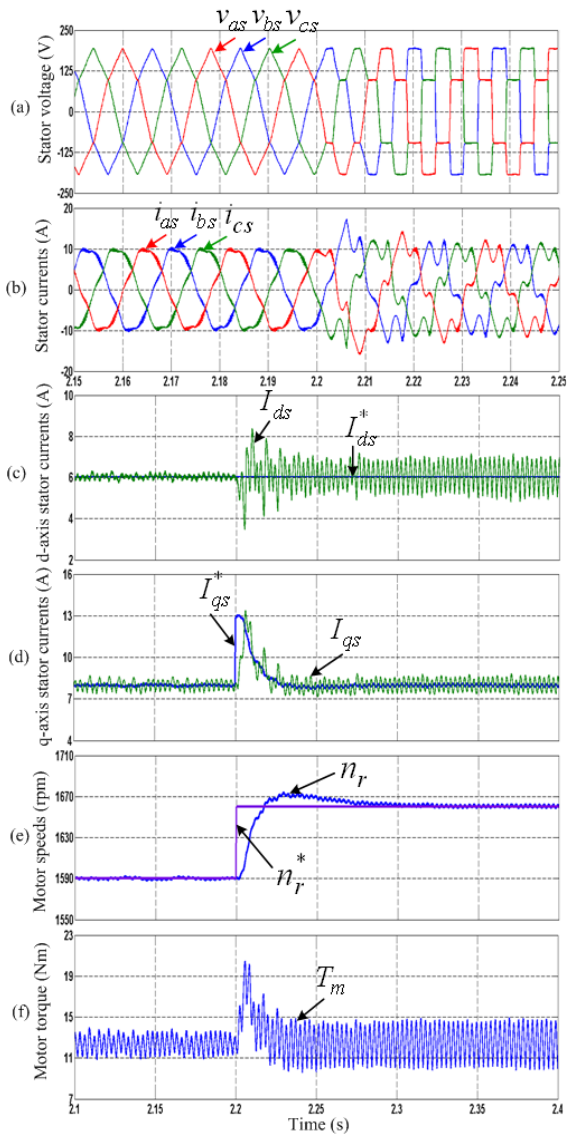

Fig. 11. Machine performance in transient state.
(a) Stator phase voltage. (b) Stator phase currents. (c) d-axis currents. (d) q-axis currents. (e) Speeds. (f) Torque.

voltages for the two methods are shown at the tops of Fig. 9(a) and (b), respectively. It can be seen that the static OVM strategy can boost the output voltage up to the six-step waveform, whereas the inverter output voltage in the case of the dynamic OVM strategy is limited up to the MI of 0.943. Due to the limitation of the output voltage in the dynamic OVM strategy, the machine cannot be controlled at a speed higher than 1,605 rpm, as shown in the bottom of Fig. 9(a). It can be seen from the bottom of Fig. 9(b) that the machine speed is controlled well up to 1,650 rpm by the proposed scheme.

Fig. 10 shows the performance of the machine under the OVM range. The stator currents, shown in Fig. 10(b), are distorted due to the presence of harmonic components of the

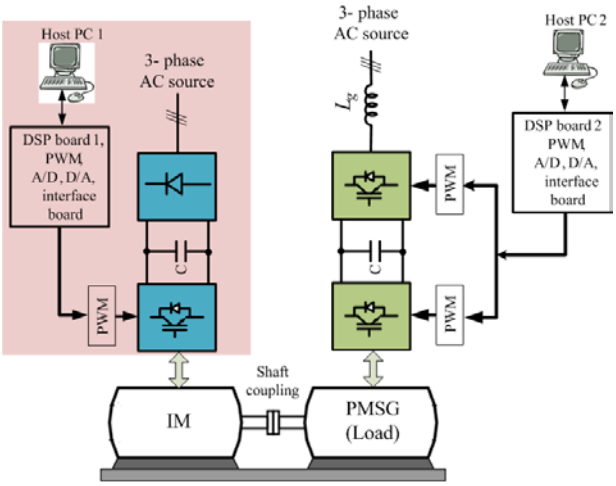

Fig. 12. Schematic diagram of experiment.

stator voltage as shown in Fig. 10(a). However, the machine operation can be kept stable. The performance of the *dq*-axis current controllers are shown in Fig. 10(c) and (d), respectively. During this operation mode, the machine speed is still controlled well. Fig. 10(e) shows that the speed control error is less than 1%. Fig. 10(f) shows the machine torque, of which the distortion is about 12.5%.

Fig. 11 shows the performance of the machine in the transient state, in which the machine speed reference is changed from 1,590 rpm to 1,660 rpm. Under this condition, the operation mode of the PWM inverter is changed from the OVM mode I to the six-step mode. The output inverter voltages are shown in Fig. 11(a). It is observed in Fig. 11(b) that the machine currents in OVM mode I are much less distorted than those of the six-step mode. The performance of the *dq*-axis machine currents are shown in Fig. 11(c) and (d), respectively. It can be seen that the *q*-axis current is increased a lot at the instant of the speed reference change. It can be seen in Fig. 11(e) that the machine speed follows its reference in 100 ms. The machine torque, as shown in Fig. 11(f), is increased quickly to accelerate the machine speed to its command.

VI. Experimental Results

A schematic diagram of the experimental setup is shown in Fig. 12. The machine parameters are the same as those in the simulation. The inverter input voltage is provided by a front-end diode rectifier, in which a 3-phase AC source of 200V/60Hz is applied to the rectifier. The discrete observer and the digital controller are based on a digital signal processor (TMS320VC33). The composite observer is designed for a nominal frequency of 60 Hz. The sampling time of the controllers and the composite observer is 100 μs .

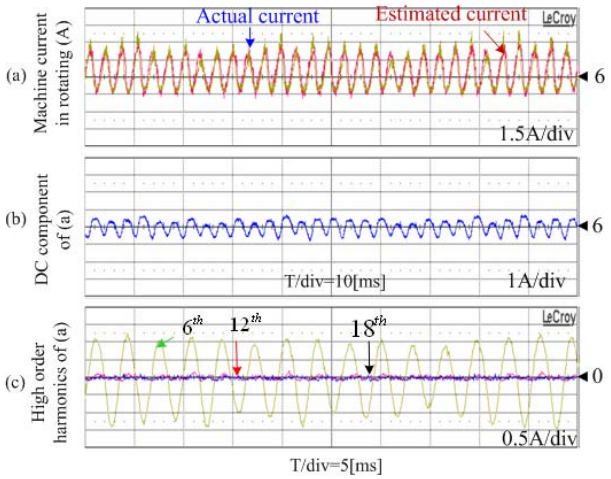

Fig. 13. Performance of composite observer for machine current estimation (MI=0.995, exp.).
(a) Actual and estimated currents. (b) Estimated DC component. (c) k·6th order harmonic components (k=1-4).

The switching frequency of the inverter is 5 kHz. A 2.68 kW permanent-magnet synchronous generator (PMSG) coupled with an IM for a load test is driven by a back-to-back converter.

The observer performance for the motor current estimation is shown in Fig. 13 for the full load operation. The estimated *d*-axis current is almost the same as the actual one, as shown in Fig. 13(a). Its DC component and the high-order harmonic components such as the 6th, 12th, 18th, and 24th are shown in Fig. 13(b) and (c), respectively.

The performance of the current controllers, between the conventional method (without harmonic current elimination) and the proposed one, are compared. Fig. 14(a) and (b) show the control performance of the two methods mentioned above, respectively. It can be seen from the top of Fig. 14(a) that the conventional PI controller produces a large ripple in the output, whereas it is much smaller for the proposed one, as shown in the top of Fig. 14(b). The middle of Fig. 14(b) shows that the response of the proposed current controller is greatly improved. The machine current follows its reference, while the ripple of the machine current is high in the conventional controller, as shown in the middle of Fig. 14(a). In addition, the bottoms of Fig. 14(a) and (b) show the machine torques for the conventional method and the proposed one, respectively. The ripple in the proposed algorithm is lower than that of the conventional one.

The performance of the machine under the OVM range of the PWM inverter is shown in Fig. 15. Fig. 15(b) shows the stator currents, which are much distorted due to the harmonic components of the stator voltage, as shown in Fig. 15(a). However, the machine operation can be kept stable. The machine current and speed are still controlled well as shown

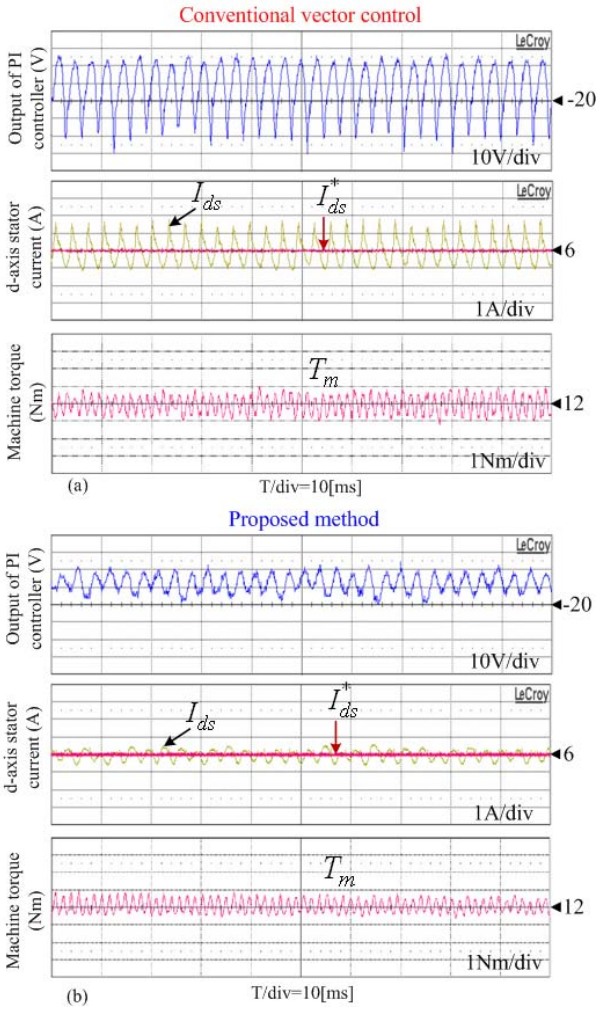

Fig. 14. Performance comparison of the PI current controllers (MI=0.98, exp.).
(a) Conventional vector control. (b) Proposed method.

in Fig. 15(c) and (d), respectively. Fig. 15(e) shows the machine torque, with a distortion is about 10%.

The transient-state operation of the machine is tested by changing the machine speed reference from 1,590 rpm to 1,660 rpm. For this condition, the operation mode of the PWM inverter is changed from OVM mode II to the six-step mode. Fig. 16(a) shows the response of the speed controller, in which the motor speed reaches its command after about 100 ms. For fast acceleration, the machine torque is increased, as shown in Fig. 16(c), by increasing the *q*-axis stator current. Fig. 16(b) shows the current control performance in the transient state, where the actual current tracks its reference quickly. The estimation performance of the composite observer for the machine current is shown in Fig. 16(d), where the estimated current follows the actual value well. The stator fluxes are shown in Fig. 16(e), and are estimated from the reconstructed stator voltages and the measured stator currents [18]. It can be seen that the machine flux is still kept

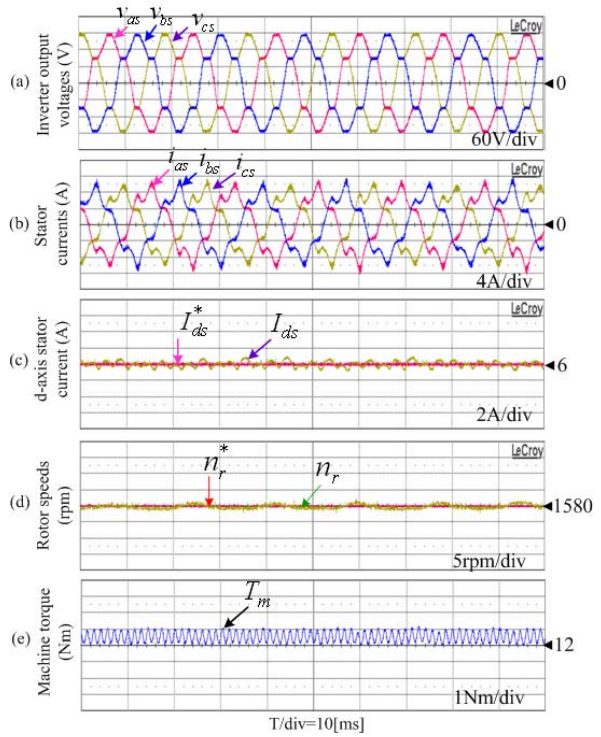

Fig. 15. Performance of the machine under OVM range (MI=0.98, exp.)
(a) Stator phase voltage. (b) Stator phase currents. (c) d-axis currents. (d) Speeds. (e) Torque.

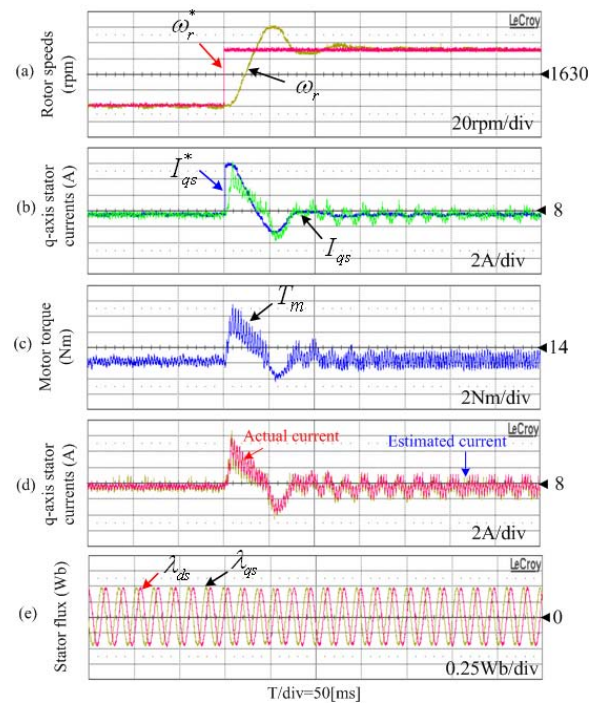

Fig. 16. Machine performance in transient state (exp.).
(a) Motor speeds. (b) q-axis stator currents. (c) Motor torque. (d) q-axis currents. (e) Fluxes.

constant at a magnitude of 0.4775 Wb during the OVM mode and the six-step mode.

VII. CONCLUSIONS

In this paper, improvements in the current control performance of vector-controlled induction motor drives has been investigated in the OVM range, where a composite observer is applied which estimates the harmonic currents. With this method, the multiples of the 6th-order harmonic components can be eliminated from the feedback current. Thus the performance of the PI current controller is kept good even though harmonic currents exist. In addition, the torque ripple of the machine becomes lower. Therefore, the machine speed ripple also becomes lower. PSIM simulation and experimental results have shown the validity of the proposed method. The proposed method is expected to be effective for the maximum utilization of the machine torque for an operating speed range that is 10.3% higher than the base speed.

ACKNOWLEDGEMENT

This research was supported by the Yeungnam University research grant in 2009.

REFERENCES

[1] D. C. Lee and G. M. Lee, "A novel overmodulation technique for space-vector PWM inverters," *IEEE Trans. Power Electron.*, Vol. 13, No. 6, pp. 1144-1151, Nov. 1998.
[2] J. Holtz, W. Lotzkat, and A. Khambadkon, "On continuous control of PWM inverters in the overmodulation range including the six-step mode," *IEEE Trans. Power Electron.*, Vol. 8, No. 4, pp. 546-553, Oct. 1993.
[3] S. Bolognani and M. Zigliotto, "Novel digital continuous control of SVM inverters in the ovemodulation range," *IEEE Trans. Ind. Applicat.*, Vol. 33, No. 2, pp. 525-530, Mar./Apr. 1997.
[4] A. M. Khambadkone and J. Holtz, "Compensated synchronous PI current controller in overmodulation range and six-step operation of space-vector modulation-based vector controlled drives," *IEEE Trans. Ind. Electron.*, Vol. 49, No. 3, pp. 574-579, Jun. 2002
[5] S. Venugopal and G. Narayanan, "An overmodulation scheme for vector controlled induction motor drives," *in Proc. IEEE PEDES*, pp. 1-6, 2006.
[6] T. H. Nguyen and D. C. Lee, "Improvement of current control in overmodulation range for vector-controlled induction machine drives," *in Proc. IEEE ICPE*, pp. 421-426, 2011.
[7] A. Tripathi, A. M. Khambadkone, and Sanjib K. Panda, "Stator flux based space-vector modulation and closed loop control of the stator flux vector in overmodulation into six-step mode," *IEEE Trans. Power Electron.*, Vol. 19, No. 3, pp. 775-782, May 2004.
[8] A. Tripathi, A. M. Khambadkone, and Sanjib K. Panda, "Direct method of overmodulation with integrated closed loop stator flux vector control," *IEEE Trans. Power Electron.*, Vol. 20, No. 5, pp. 1161-1168, Sep. 2005.

[9] A. Tripathi, A. M. Khambadkone, and S. K. Panda, "Dynamic control of torque in overmodulation and in the field weakening region," *IEEE Trans. Power Electron.*, Vol. 21, No. 4, pp. 1091-1098, Jul. 2006.
[10] T. H. Nguyen, T. L. Van, D. C. Lee, J. H. Park, and J. H. Hwang, "Control mode switching of induction machine drives between vector control and V/f control in overmodulation range," *Journal of Power Electronics*, Vol. 11, No. 6, pp. 846-855, Nov. 2011.
[11] J. K. Seok, J. S. Kim, and S. K. Sul, "Overmodulation strategy for high-performance torque control," *IEEE Trans. Power Electron.*, Vol. 13, No. 4, pp. 786-792, Jul. 1998.
[12] B. H. Bae and S. K. Sul, "A novel dynamic overmodulation strategy for fast torque control of high-saliency-ratio AC motor," *IEEE Trans. Ind. Applicat.*, Vol. 41, No. 4, pp. 1013-1019, Jul./Aug. 2005.
[13] D. M. Lee, J. W. Jung, and S. S. Kwak, "Simple space vector PWM scheme for 3-level NPC inverters including the overmodulation region," *Journal of Power Electronics*, Vol. 11, No. 5, pp. 688-696, Sep. 2011.
[14] C. T. Chen, *Linear System Theory and Design*. New York: Oxford University Press, 1999.
[15] K. Selvajyothi and P. A. Janakiraman, "Extraction of harmonics using composite observers," *IEEE Trans. Power Del.*, Vol. 23, No. 1, pp. 31-40, Jan. 2008.
[16] K. Selvajyothi and P. A. Janakiraman, "Reduction of voltage harmonics in single phase inverters using composite observers," *IEEE Trans. Power Del.*, Vol. 25, No. 2, pp. 1045-1057, Apr. 2010.
[17] S. K. Sul, *Control of electric machine drive systems*, New Jersey: Wiley, Chap. 5, 2011.
[18] Peter Vas, *Sensorless vector and direct torque control*, Oxford Science Publications, Chap. 4, 1998.

Thanh Hai Nguyen was born in Dong Thap, Viet Nam in 1980. He received his B.S. in Engineering from the Technology University of Ho Chi Minh City, Viet Nam, in 2003, and his M.S. in the Department of Electrical Engineering, Yeungnam University, Gyeongbuk, Korea, in 2010, where he is currently working toward his Ph.D. He was an Assistant Lecturer in the College of Technology, Can Tho University, Viet Nam, in 2003. His current research interests include power converters, machine drives, and wind power generation.

Dong-Choon Lee received his B.S., M.S., and Ph.D. in Electrical Engineering from Seoul National University, Seoul, Korea, in 1985, 1987, and 1993, respectively. He was a Research Engineer with Daewoo Heavy Industry from 1987 to 1988. Since 1994, he has been a Faculty Member in the Deptartment of Electrical Engineering, Yeungnam University, Gyeongbuk, Korea. Currently, he is serving as a Publication Editor for the Journal of Power Electronics, Korean Institute of Power Electronics, Korea. As a Visiting Scholar, he joined the Power Quality Laboratory, Texas A&M University, College Station, USA, in 1998, the Electrical Drive Center, University of Nottingham, U.K., in 2001, and the Wisconsin Electric Machines and Power Electronic Consortium, University of Wisconsin, Madison, USA, in 2004. His current research interests include ac machine drives, control of power converters, wind power generation, and power quality.